Cyclic mimetics of kinase-inhibitory region of Suppressors of Cytokine Signaling 1: Progress toward novel anti-inflammatory therapeutics

Sara La Manna [a, b], Laura Lopez-Sanz [b, c], Susana Bernal [b, c], Sara Fortuna [d], Flavia A. Mercurio [e], Marilisa Leone [e], Carmen Gomez-Guerrero [b, c], Daniela Marasco [a, *]

[a] Department of Pharmacy - University of Naples "Federico II", 80134, Naples, Italy
[b] Renal and Vascular Inflammation Group, Instituto de Investigacion Sanitaria-Fundacion Jimenez Diaz (IIS-FJD), Autonoma University of Madrid (UAM), 28040, Madrid, Spain
[c] Spanish Biomedical Research Centre in Diabetes and Associated Metabolic Disorders (CIBERDEM), 28040, Madrid, Spain
[d] Department of Chemical and Pharmaceutical Sciences, University of Trieste, 34127, Trieste, Italy
[e] Institute of Biostructures and Bioimaging - CNR, 80134, Naples, Italy

ARTICLE INFO

Accepted 8 May 2021

Keywords:
Mimetic peptides
Cytokine signaling
JAK/STAT
SOCS1
Oxidative stress
Inflammation

ABSTRACT

Herein we investigated the structural and cellular effects ensuing from the cyclization of a potent inhibitor of JAK2 as mimetic of SOCS1 protein, named PS5. The introduction of un-natural residues and a lactam internal bridge, within SOCS1-KIR motif, produced candidates that showed high affinity toward JAK2 catalytic domain. By combining CD, NMR and computational studies, we obtained valuable models of the interactions of two peptidomimetics of SOCS1 to deepen their functional behaviors. Notably, when assayed for their biological cell responses mimicking SOCS1 activity, the internal cyclic PS5 analogues demonstrated able to inhibit JAK-mediated tyrosine phosphorylation of STAT1 and to reduce cytokine-induced proinflammatory gene expression, oxidative stress generation and cell migration. The present study well inserts in the field of low-molecular-weight proteomimetics with improved longtime cellular effects and adds a new piece to the puzzled way for the conversion of bioactive peptides into drugs.

1. Introduction

Suppressors of Cytokine Signaling (SOCS) proteins' family consists of eight proteins, namely, cytokine-inducible SH2-containing protein (CIS) and SOCS 1–7 [1–3]. Although the biological roles of SOCS 4–7 are still not well understood, CIS and SOCS 1–3 are well characterized as cytokine-inducible negative feedback regulators of JAK/STAT signaling [4]. Besides this regulatory function, SOCSs have other roles in immunologic cascades [5] as recently demonstrated in bone resorption processes [6]. Noticeably SOCS proteins exert a major role in innate immune responses caused by viral infections and in assisting viruses to escape immunity [7,8].

All SOCS members present a modular organization: i) a variable N-terminal region, ii) a central Src Homology 2 (SH2) domain, and iii) a conserved C-terminal domain (SOCS box) [9]. Only SOCS1 and 3 bear the kinase inhibitory region (KIR) motif in the N-terminal part, but they have different mechanisms of action. For instance, SOCS3, besides interacting with JAK2, simultaneously interacts with the cytokine receptor [10] without affecting JAK2 phosphorylation. Conversely, SOCS1 binds JAK2 also when unphosphorylated [11] and represses its phosphorylation unassisted by receptors [12]. SOCS1 regulates cellular pathways modulated by different cytokines as type I and II interferon (IFN) [13,14], interleukin (IL)-2 [15], IL-12/23 [16], and IL-6 [17]. Indeed, its overexpression reduces the expression of pro-inflammatory genes such as the Intercellular Cell Adhesion Molecule-1 (*ICAM-1*), the C-X-C motif chemokine ligands (*CXCL*) 10 and 9, and the C-C motif chemokine ligands 2 and 5 (*CCL2, CCL5*) [18], and enhances the deleterious effects of IFNs in experimental autoimmune encephalitis, a model of Multiple Sclerosis [19]. Deficiency in SOCS1 ($SOCS1^{-/-}$) implies fatal inflammatory diseases dependent on type II IFN [20,21], whereas SOCS1 haploinsufficiency causes a dominantly inherited predisposition to early onset autoimmune diseases related to cytokine hypersensitivity of immune cells [22].

SOCS1 acts as a direct inhibitor of JAK1, JAK2, TYK2, but not of JAK3. Structural studies confirmed that SOCS1 blocks the substrate

* Corresponding author.
E-mail address: daniela.marasco@unina.it (D. Marasco).

binding groove on JAKs, acting as a pseudosubstrate. In the crystal structure of the complex SOCS1 binds to JAK1 using both SH2 and KIR domains and displays minor structural changes upon JAK1 binding, the main difference appears that KIR becomes ordered in the JAK-bound state [11]. The recognition between SOCS1 and JAK1 is mediated by a continuous six residues segment of KIR (His^{54} to Arg^{59}) where each amino acid is involved both in polar and/or hydrophobic interaction: His^{54} is located between two planar side chains (His^{885} and Pro^{1044}) from JAK1, while Phe^{55} is the P+1 residue of the pseudosubstrate of the kinase and both His^{54} and Phe^{55}, together with Phe^{58} form most of hydrophobic interactions that wedge KIR between the activation loop and the αG helix of JAK1 [11].

The peptide covering the fragment 52–67 of SOCS1 KIR demonstrated able to inhibit STAT activation by Th1 and Th17 cytokines in leukocytes, to suppress the activation and migration of vascular cells and macrophages *in vitro* [23], to reduce the expression of pro-inflammatory cytokines in atherosclerotic plaques [24], to improve diabetic kidney disease in mouse models of type 1 and type 2 diabetes by reducing renal inflammation, oxidative stress and fibrosis [25–27], to suppress chronic intraocular inflammatory disease (uveitis) [27–29] and, very recently, to have protective effects in experimental abdominal aortic aneurysm [30].

Previous studies aimed at identifying new mimetics of SOCS1 KIR allowed us to identify a lead-compound, named PS5, able to bind JAK2 more efficiently than KIR and to prevent cytokine-induced activation of STAT and downstream inflammatory and immune responses [31–33]. Very recently we have assessed the antioxidant and atheroprotective properties of PS5 in a mouse model of atherosclerosis, thus highlighting how mimetics of SOCS1 can be considered hopeful therapeutics [34].

Herein, we designed and tested new PS5 analogues containing a lactam bridge between side chains (hence the name of internal cycles PS5) as novel peptidomimetics of SOCS1. We investigated their conformational properties through Circular Dichroism (CD) and Nuclear Magnetic Resonance (NMR) and their affinities to JAK2 through microscale thermophoresis (MST). The anti-inflammatory and antioxidant effects were assessed in vascular smooth muscle cells (VSMCs) and macrophages, two cell cultures critically involved in cardiovascular diseases.

2. Results and discussion

2.1. Design of internal cyclic PS5 analogues

A few years ago, on the basis of studies carried out on KIR peptide (SOCS1 52–67 fragment) (Table S1, Fig. 1A and Scheme S1) we identified the linear PS5 sequence [32]. It was obtained by i) restricting KIR to 52–61 fragment (named New KIR, Scheme S1) upon Ala-scan of the entire 52–67 sequence, and ii) through the screening of "combinatorial focused libraries" in Positional Scanning format [35–37], carrying the mutations His^{54}/Cys(Acm), Phe^{55}/Arg and Arg^{56}/Gln (Table S1, Fig. 1B, and Scheme S1). No structural details were obtained for linear PS5 peptide due to its intrinsic flexibility. To overcome this problem, we firstly designed cyclic compounds by introducing a disulfide bridge at the extremities, but they did not provide promising results and were no further investigated [33]. Herein we conceived a novel 10 amino acids cycle obtained through a lactam bridge between side chains of aspartic acid, naturally found at position 52, and a lysine inserted at position 60 in place of Ser, that, in turn, revealed not so crucial for the affinity, in the Ala-scan analysis of the entire KIR peptide (Scheme S1) [32]. The novel cyclic compound was named internal cyclic PS5. Furthermore, with the aim to limit both the flexibility of the cycle [38] and to enhance proteolytic stability of peptide [33], we also investigated the same compound bearing the non-natural L-1-naphthylalanine in place of Phe^{58}; this compound is herein reported as internal cyclic PS5 Nal1. The chemical structures of these two new PS5 analogues are reported in Fig. 1C–D.

2.2. Binding affinities and conformational properties of internal cyclic PS5 analogues

PS5 internal cyclic analogues were assayed for their ability to bind to JAK2 catalytic domain through MST experiments (Fig. 2A–B). For both cyclic peptides, a dose-response curve was observed and the signal reach saturation (thermophoretic traces and capillary shapes are reported in Fig. S1). The fitting of experimental data provided similar K_D values of 44 ± 6 μM for internal cyclic PS5 (Figs. 2A) and 35 ± 1 μM for internal cyclic PS5 Nal1 (Fig. 2B).

To evaluate the conformational properties of designed peptidomimetics, CD and NMR spectroscopic studies were carried out (Fig. 2C–D). Both analogues do not show canonical profiles with a prevalent random contribution due to fact that absolute minima are located at $\lambda \leq 200$ nm. Moreover, in both cases "aromatic" bands are present: a negative shoulder for PS5 internal cycle (Fig. 2C) and a more pronounced positive band for internal cyclic PS5 Nal1 (Fig. 2D), centered at 230 nm. For both compounds, the evidence of aromatic contribution to the Cotton effect is likely due to the presence of a cyclic structure, indeed these bands are absent in the linear versions of these peptidomimetics [33]. In detail, internal cyclic PS5 Nal1 also presents a shoulder at 222 nm indicative of a major helical content for Nal1 containing sequence. On the other hand, the positive band at 232 nm for this compound is due to an exciton effect [39] since it is lost upon temperature increase in the range of 20–95 °C (Figure S2 A). By comparing CD spectra at different temperatures, and after cooling back the sample to 20 °C, this spectral change appeared reversible (Figure S2 B).

The conformational properties of internal cyclic PS5 and PS5 Nal1 compounds were investigated by means of NMR in H_2O/D_2O. To this aim, different 2D [^{1}H, ^{1}H] NMR spectra were registered, and the analysis of TOCSY [40] and ROESY [41] experiments allowed to obtain complete peptide proton resonance assignments (Tables S2–S3 and Fig. S3). Inspection of NOESY [42] and ROESY spectra indicated that both peptides do not assume a rigid structure. In fact, analysis of ROEs patterns (Fig. S4) in which sequential H_N-H_Ni+1 and Hα-H_Ni+1 contacts prevail, pointed out the absence of canonical secondary structure elements [43]. Complete 3D solution structure calculations were conducted with the software CYANA [44] and confirmed an intrinsic flexibility of both cycles.

NMR structures were next subjected to an unrestrained energy minimization procedure (Fig. S5) after which only 9/20 conformers of internal cyclic PS5 and Nal1 assumed distorted 3_{10} helical turns.

A cluster analysis of minimized structures was carried out with the software Chimera [45,46] (Fig. 3 and Table S4). Clusterization stressed also out a certain conformational variability: indeed it provided, for internal cyclic PS5, 12 clusters of conformational related subfamilies (Fig. 3 A, B, C), the two most populated ones containing 4 models (Fig. 3 B-C, and Table S3), while internal cyclic PS5 Nal1 conformers can be grouped into 9 clusters, 5 of them represented by only 1 model (Table S3), and the two most populated ones containing each 6 and 5 conformers, respectively (Fig. 3D–F).

2.3. Computational analysis of JAK2/internal cyclic PS5 complexes

To complete structural investigation on internal cyclic PS5 analogues docking studies were carried out. To this purpose, a JAK2/

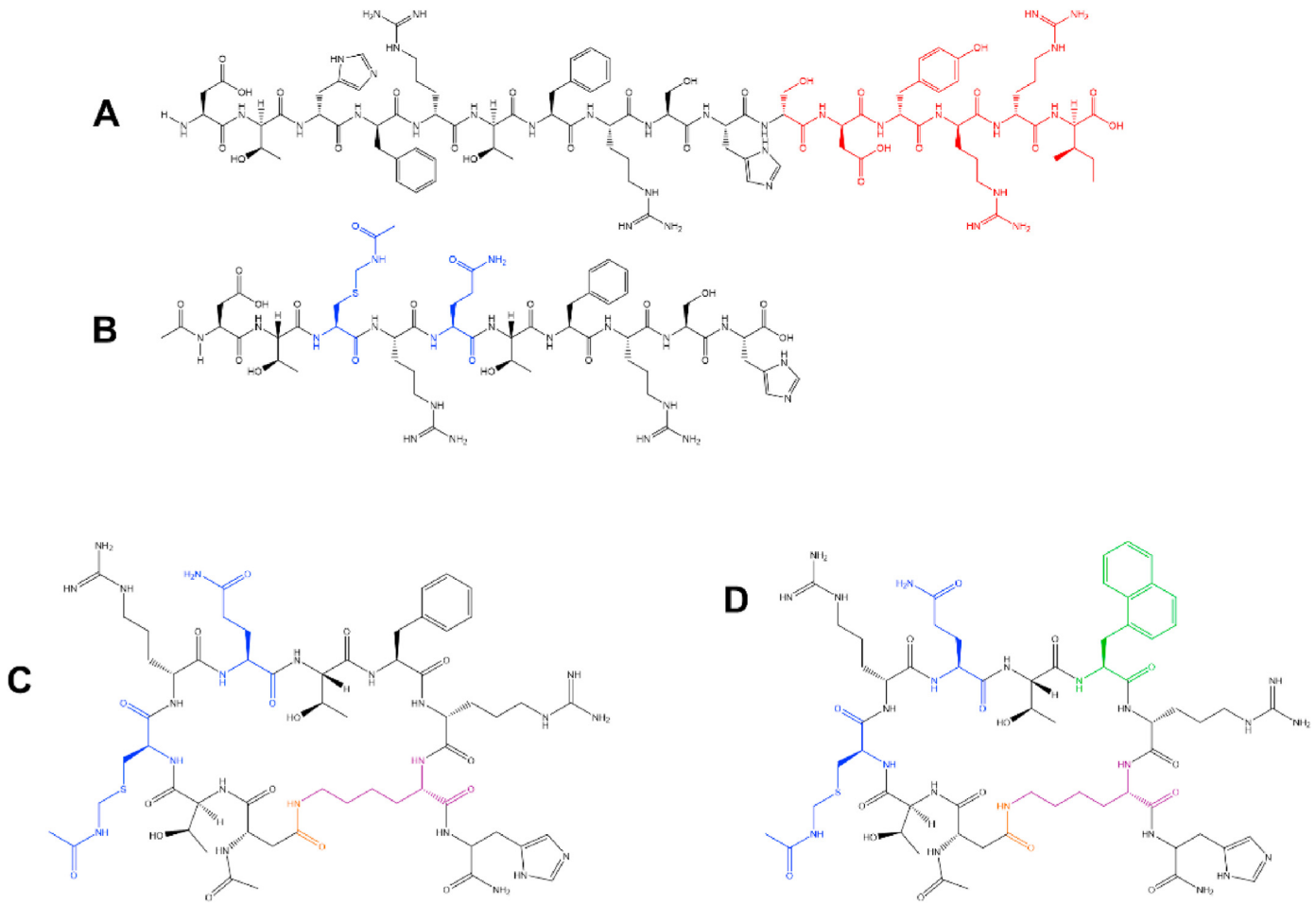

Fig. 1. Chemical structures of A) KIR, B) PS5, C) Internal cyclic PS5, D) Internal cyclic PS5 Nal1. In red residues removed from KIR sequence to generate PS5; in blue the two non-native residues (Cys(Acm) and Gln) deriving from combinatorial screening of PS-focused peptide libraries; in green the substitution Nal1/Phe58; in purple the substitution of Ser60/Lys; in orange the lactam bridge between the side chains of aspartic acid and lysine.

SOCS1 model was built by homology modelling to delineate the KIR binding site on JAK2. The crystal structure of the complex JAK1/SOCS1 (PDB: 6C7Y [47]) was employed as template since JAK1 covers the 94% of the JAK2 sequence with 56% identity and the crystal structure of JAK2 was also available (PDB: 3FUP [48]). JAK2 and JAK1 were then superposed to build JAK2/SOCS1 (Figure S6 A-B), and then the JAK2/KIR complex was extracted (Fig. S6C), allowing to identify the KIR-SOCS1 binding site on JAK2 that is fully consistent with previous models [49]. Both cyclic peptides were docked to the SOCS1 KIR binding site on JAK2. Internal cyclic PS5 Nal1 lowest docked configuration scored −5.0 kcal/mol with AutoDock Vina (Fig. S6E) while internal cyclic PS5 scored −5.1 kcal/mol (Fig. S6D). The docking data indicate that both compounds can actually bind their target site on JAK2 with comparable strengths, as already highlighted by MST. Docking results further suggest that internal cyclic PS5 Nal1 (Fig. S7B) tends to explore different configurations with root mean square deviation (RMSD) up to 0.44 nm with respect to the optimum pose, while internal cyclic PS5 docking poses are similarly oriented having RMSD below 0.16 nm (Fig. S7A). The lowest docked configurations of Figs. S6D–E were used as starting point for the subsequent molecular dynamics (MD) simulations.

Due to the intrinsic flexibility of cyclic analogues, to explore their conformational space we run 150ns of MD simulation on the optimum internal cyclic PS5/JAK2 complexes. MD simulation explores lowest scoring poses among those obtained by docking reaching −16.6 AutoDock Vina score for internal cyclic PS5 at 57.7ns and −14.4 for internal cyclic PS5 Nal1 at 95.5ns (Fig. 4A–B). These are metastable states and both systems relax towards binding scores (−11.4 ± 1.7 and −10.6 ± 1.3 kcal/mol) once again comparable and indicate low μM range for dissociation constants.

The new poses are the result of minor peptide rearrangements and larger protein backbone rearrangements as evident from RMSD profiles in the simulation time (Fig. 4C–D). The protein rearrangement upon binding is particularly evident in the internal cyclic PS5/JAK2 complex with the RMSD reaching 2.0 nm; noticeably JAK2 radius of gyration does not change upon binding (Fig. 4E–F). The root mean squared fluctuation (RMSF) confirm this observation as only the flexible loop interconnecting two helices (from amino acid 100 to 125) of JAK2 reaches values above 0.5 nm over the last 100ns of the simulation (Fig. 4G–H).

For an accurate estimation of the binding energy, we performed a molecular mechanics/Poisson-Boltzmann solvent-accessible surface area (MM/PBSA) analysis on the last 100ns of each trajectory (Fig. 4I–J). The van der Waals contributions are equivalent for the two cyclic analogues, but the favorable electrostatic interactions appeared almost doubled for internal cyclic PS5, that presents an opposing larger polar solvation energy contribution, that appears reduced in cyclic PS5 Nal1. In the evaluation of the contribution of single amino acid to the binding energy (Fig. 4 K, L), for both

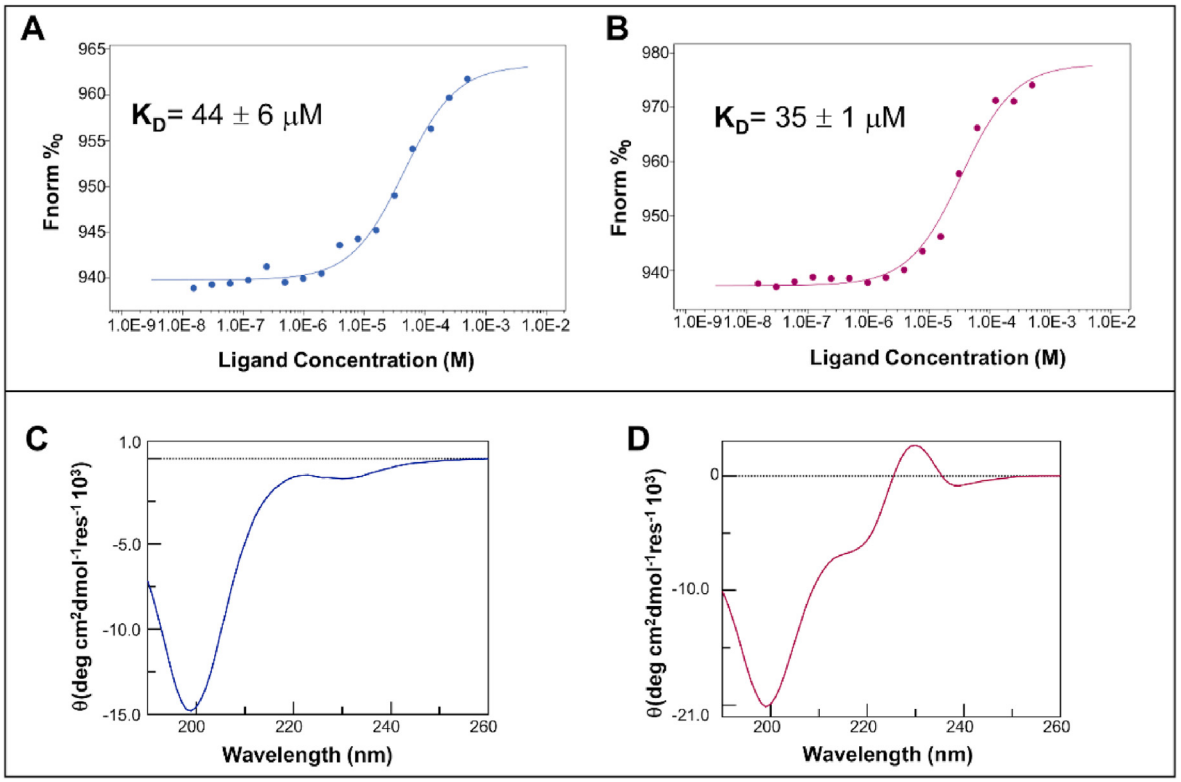

Fig. 2. Binding isotherms for MST signals versus peptide concentrations. Cyclic PS5 analogues were employed with a serial dilution (1:1) by preparing 16 samples on average of the following stock solutions 1 mM, in labeling buffer at pH 7.5 (A) internal cyclic PS5 and (B) internal cyclic PS5 Nal1. CD spectra of C) internal cyclic PS5 and D) internal cyclic PS5 Nal1.

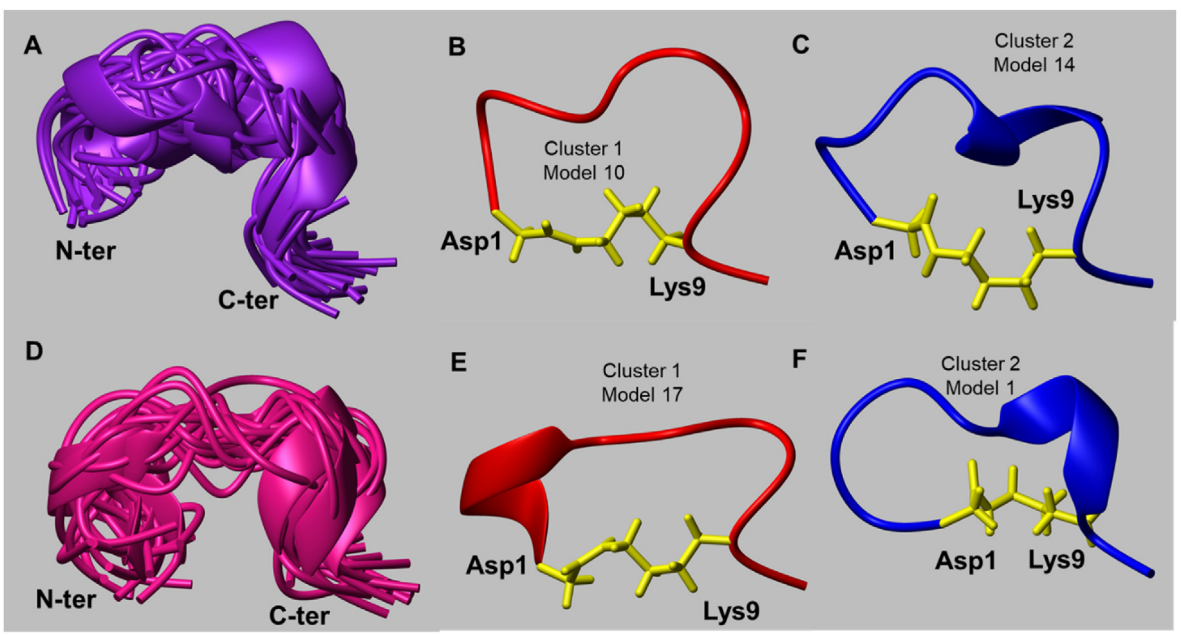

Fig. 3. NMR structures of cyclic PS5 analogues. Internal cyclic PS5: (A) twenty calculated conformers superimposed on the backbone atoms (ribbon representation, $RMSD_{bb}$ = 1.68 Å). (B, C) Representative models from most populated clusters. Internal cyclic PS5-Nal1: (D) 20 NMR minimized conformers superimposed on the backbone atoms in ribbon representation ($RMSD_{bb}$ = 1.77 Å). (E, F) Representative models from the most populated clusters. Peptide cyclization is highlighted in yellow.

analogues long range interactions are mainly responsible of the bound state of ligands to the target (Fig. 4 K, N), but important differences are observed at short range. For internal cyclic PS5 peptide, Phe[7] strongly interacts with Glu[50] and Glu[51] of JAK2 and forms H-bonds with the backbone oxygen of Leu[187] and the backbone nitrogen of Lys[172], respectively (Fig. 4 O). These attractive interactions are counterbalanced by strong repulsive interactions between the internal cyclic PS5 peptide and JAK2 through Arg[54]

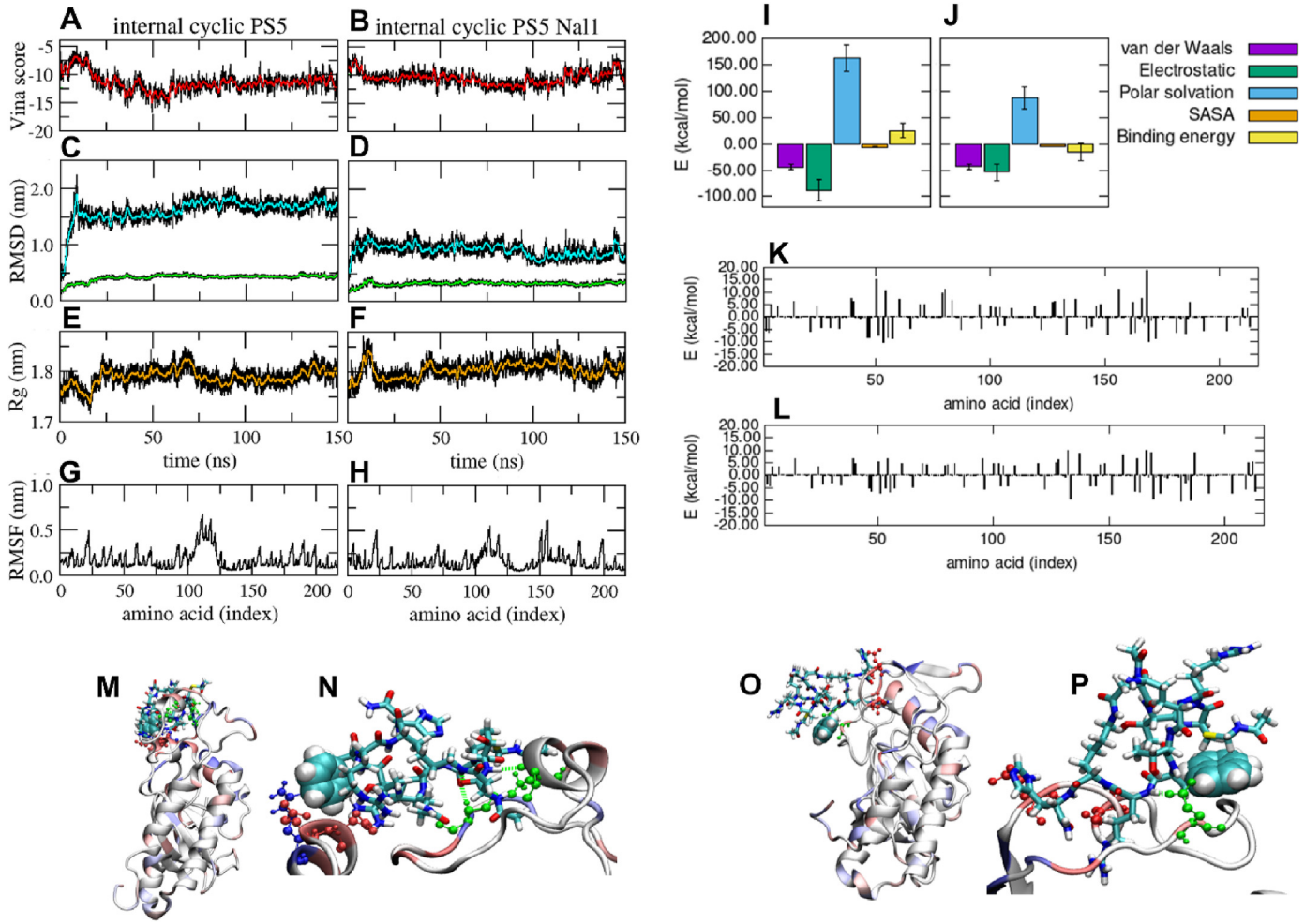

Fig. 4. Molecular dynamic analysis. Internal cyclic PS5 (A, C, E, G) and internal cyclic PS5 Nal1 (B, D, F, H). (A-B) AutoDock Vina score along the MD trajectory (black solid line), and its running average (red solid line) (C-D) peptides RMSD in the frame of the protein backbone (black) and its running average (green) and protein backbone RMSD together with its running average (cyan); (E-F) backbone radius of gyration (black) and its running average (orange); (G-H) protein backbone RMSF calculated over the last 100 ns (black). MM/PBSA analysis over the last 100ns of the molecular dynamics trajectory: amino acids contribution to the total binding energy for (I) internal cyclic PS5 and (J) internal cyclic PS5 Nal1; details of the contributions of each amino acid for (K) internal cyclic PS5 and (L) internal cyclic PS5 Nal1; configurations with their lowest VINA scores (M) for internal cyclic PS5 at 57.7ns and (O) for internal cyclic PS5 Nal1 at 95.5ns; close ups on (N) internal cyclic PS5 and (P) internal cyclic PS5 Nal1 with highlighted amino acids with positive (shades of blue) and negative (shades of red) contribution to the binding energy, hydrogen bonds and involved JAK2 amino acids are highlighted in green, Phe and Nal1, at position 7, are highlighted with their van der Waals spheres.

and Lys^{172} (15.3 and 18.6 kcal/mol respectively). For internal cyclic PS5 Nal1 at short range Glu^{185} and Glu^{189} strongly contributes to the binding which is further strengthened by a H-bond with Glu^{176} (Fig. 4 P).

2.4. Characterization of the inhibitory effects of internal cyclic PS5 analogues on JAK/STAT pathway mediated responses in cultured cells

Prior to evaluate the biological effects of PS5 analogues on cell-based assays, we comparatively analyzed their stability against enzymatic degradation in serum (Fig. S8). Interestingly, during the first 24 h, the cyclic structure was able to stabilize both analogues with respect to linear PS5, the latter showing a degradation level of ~50%. Then, as expected, the reduction of integrity of internal cyclic PS5 Nal1 was significantly lower (~20%) with respect to internal cyclic PS5 (~40%) for the presence of the non-natural Nal1 residue. This tendency was confirmed at 42 h, when the residual concentration of internal cyclic PS5 Nal1 was still at ~40%, while the other peptides appeared almost completely degraded.

To allow and evaluate cell penetration, PS5 analogues were covalently attached to the cell-penetrating peptide covering the fragment 48–60 of the HIV Tat and the fluorophore TAMRA. Their cellular uptake was analyzed during time and related confocal microscopy images were collected (Fig. S9) highlighting how both cyclic peptidomimetics showed an efficient and similar uptake and a predominant cytoplasmic distribution. Internal cycle PS5 Nal1 demonstrated more stable over time with respect to internal cycle PS5 also in a cellular context, thus confirming *in vitro* serum assays.

We next investigated whether PS5 analogues influence cell viability, proliferation and migration. MTT colorimetric assays revealed no cytotoxic activity of PS5 and its analogues in cultured VSMCs under both basal (medium with FBS, 0.5%, 6–24 h) and growing (medium with FBS, 10%, 24 h) conditions (Figs. S10A–B). Furthermore, in the wound-healing assay cyclic PS5 analogues significantly diminished the migration of VSMCs induced by a combination of the inflammatory cytokines IFNγ and IL6 (Figs. S10C–D). This ability was already demonstrated by KIR [27] and PS5 [34] sequences. Both PS5 analogues exhibited an anti-migratory activity over 45 h that derives from a combined

inhibitory effect on cell proliferation and migration. In line with serum stability, at 45 h internal cyclic PS5 Nal1 appeared a more potent inhibitor of wound repair compared to internal cyclic PS5 likely because of its greater intracellular stability.

Immunofluorescence and Western blot experiments were carried out to check the ability of the new analogues to mimic the biological activity of natural SOCS1 protein as JAK/STAT pathway regulator. Confocal immunofluorescence in VSMC (Fig. 5A–E) revealed that cytokine-induced STAT1 phosphorylation, and nuclear translocation was inhibited to a similar extent (~65%) by both PS5 analogues.

These results were confirmed by Western blot analysis, showing a significant decrease of STAT1 phosphorylation levels in cells pretreated with PS5 compounds, but not the negative control (NC), before cytokine stimulation (Fig. 5F). Interestingly, the ability of the new analogues to mimic the biological activity of SOCS1 protein was also confirmed by the significant inhibition (but not total) of JAK2 phosphorylation levels, as shown in Fig. 5F. Furthermore, as downstream effects of the specific inhibition of JAK/STAT signaling, we observed a reduced mRNA expression of inflammatory genes such as *Ccl2, Ccl5* and *Cxcl0* chemokines in VSMCs (Fig. 5G–I). Similar inhibitory effects were also observed in macrophage cell line RAW264.7 (Fig. S11). These results indicate that the fine-tuning of JAK2's activity is essential for cell homeostasis and a partial modulation of JAK/STAT pathway might be of potential value in the treatment of vascular inflammatory diseases.

Finally, the effect of PS5 analogues on oxidative stress was evaluated by measuring intracellular $O_2^{\bullet-}$ levels in cytokine-stimulated VSMCs and RAW264.7 cells. Dihydroethidium (DHE) confocal imaging data (Fig. 6A–B) clearly showed that pretreatment with the peptidomimetics resulted in a significant decrease of $O_2^{\bullet-}$ production in both cell types. This antioxidant effect of PS5 analogues was corroborated by PCR expression analysis which showed a strong reduction in the gene expression of NADPH oxidases *(Nox1* and *Nox4*) (Fig. 6D) and significant upregulation of antioxidant genes superoxide dismutase 1 (*Sod1*) and catalase (*Cat*) (Fig. 6C).

3. Conclusion

In recent decades, cyclic peptidomimetics attracted great attention in drug discovery processes since they present more rigid conformations in comparison with linear peptides and often present more favorable pharmacological profiles. In addition, they result the most suitable compounds for modulating protein–protein interactions (PPIs), which often are considered as "undruggable targets" in traditional drug screenings based on small molecules [50,51].

This study confirmed the crucial role exerted by KIR-SOCS1 in inhibitory functions of the entire protein on JAK/STAT pathway: it presents results on the investigations of two novel constrained proteomimetics bearing un-natural amino acids and a cyclic structure, designed on the basis of the linear lead compound PS5 [31–33]. For both compounds docking and MD data indicate that van der Waals and electrostatic interactions mainly drive the recognition between JAK2 and internal PS5 cycles. Binding experiments indicate that the substitution Phe/Nal1 slightly enhances the affinity of PS5 internal cycles toward the catalytic domain of

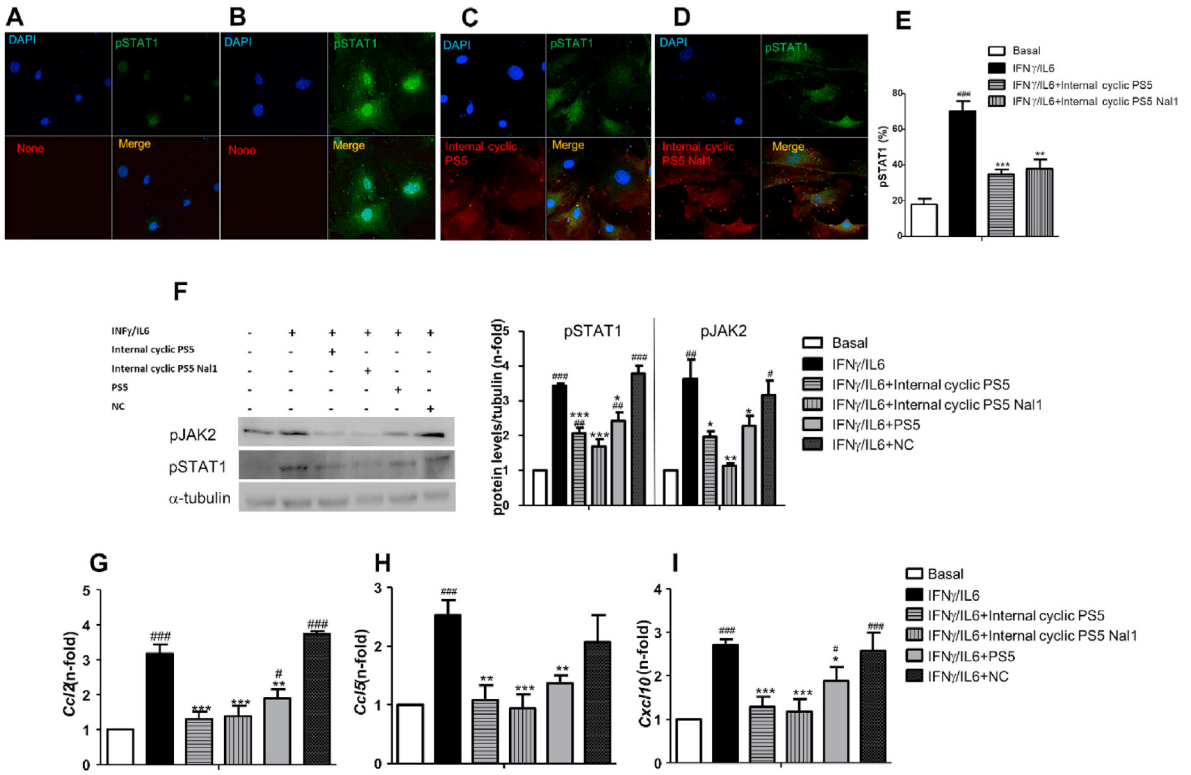

Fig. 5. Inhibitory effects of internal cyclic PS5 analogues on STAT1 activation and target gene expression. (A-D) Representative confocal images (n = 3 independent experiments) of cells under basal conditions (A), stimulated with IFNγ+IL6 (B), IFNγ+IL6/Internal cyclic PS5 (5 μM) (C), and IFNγ+IL6/Internal cyclic PS5 Nal1 (5 μM) (D) (red, PS5 analogues; green, pSTAT1; blue, DAPI stained nuclei). (E) Quantification of pSTAT1 fluorescence percentages expressed as mean ± SEM. (F) Western blot analysis of pJAK2, pSTAT1 and α-tubulin (loading control) in mouse VSMCs stimulated with IFNγ+IL-6 in absence or presence of both internal cycles, PS5 and NC peptide. Shown are representative immunoblots (F) and normalized densitometry data expressed as fold increases versus basal conditions (arbitrary set as 1). (G-I) The mRNA expression levels of Ccl2 (G), Ccl5 (H) and Cxcl10 (I) analyzed by real time PCR were normalized to 18S and expressed as fold increases over basal conditions (n = 4–5 independent experiments). Mean ± SEM ($^{\#}P < 0.05$, $^{\#\#}P < 0.01$, $^{\#\#\#}P < 0.001$ vs basal; $^{*}P < 0.05$, $^{**}P < 0.01$, $^{***}P < 0.001$ vs cytokines).

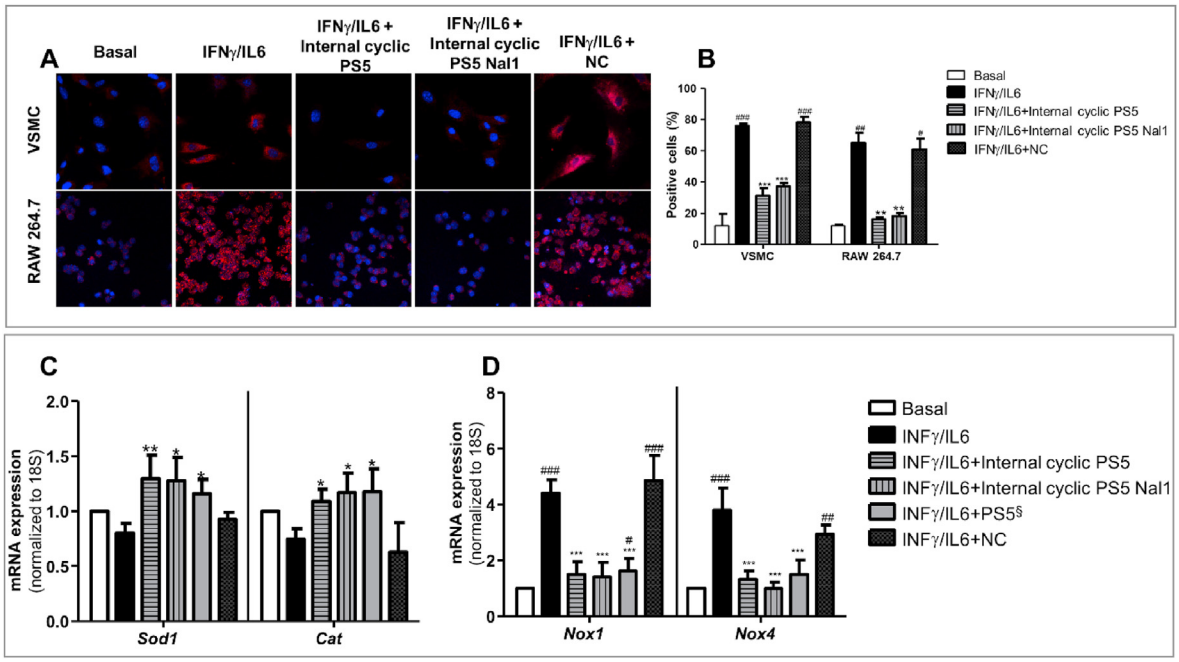

Fig. 6. Effects of internal cyclic peptides on oxidative stress. (A) Representative confocal images of intracellular $O2^{\bullet-}$ (red, DHE staining; blue, DAPI nuclear staining) in VSMCs and RAW264.7 cells stimulated with cytokines in the presence or absence of PS5 analogues and NC. (B) Quantification of peptides activity based on DHE fluorescence intensity. Results are presented as mean ± SEM of n = 3 independent experiments. (C-D) Real time PCR analysis of the mRNA expression levels of antioxidant (C) and pro-oxidant (D) enzymes in VSMCs pretreated with peptidomimetics before cytokine stimulation. Values were normalized to 18S and expressed as fold increases over basal condition. Results are presented as mean ± SEM of n = 5 experiments. $^{\#}P < 0.05$, $^{\#\#}P < 0.01$ and $^{\#\#\#}P < 0.001$ vs basal; $^{*}P < 0.05$, $^{**}P < 0.01$ and $^{***}P < 0.001$ vs cytokines.

JAK2 suggesting a major role exerted by aromatic moieties in the formation of the complex. This feature was confirmed also by i) CD studies that showed an aromatic effect in PS5 Nal1 internal cycle not observable for Phe derivative and ii) computational analysis where the opposing contribution to the interaction of polar solvation energies is weaker for PS5 Nal1 internal cycle and appeared counterbalanced by the attractive forces. These differences are more evident in cellular contexts, where the cyclic structure along with the un-natural Nal1 residue allow prolonged effects of the compound for its greater resistance to proteases degradation. However, both PS5 cyclic analogues demonstrated to mimic SOCS1 at a greater extend with respect to linear PS5in the reduction of STAT1 phosphorylation as well as in the downstream suppression of pro-inflammatory genes. In detail, in atherosclerosis relevant cells, the Nal1 containing cycle exhibited longtime anti-migratory effects that could be of great importance to limit plaque formation [52,53]. In addition, PS5 cyclic compounds showed indirect antioxidant properties through the regulation of redox balance genes, as already demonstrated recently for PS5 molecule [34], and in line with the reported effects of SOCS1/3 proteins in the modulation of pro-oxidant and antioxidant pathways in different cells [25,54,55]. Future studies in animal models are required to confirm the encouraging beneficial effects of these novel agents in cardiovascular diseases. In conclusion, presented data provide invaluable tools for the design of novel and specific JAKs' inhibitors for therapeutic applications in different inflammatory diseases.

4. Experimental

4.1. Peptide synthesis and cyclization

Peptides analyzed in this study were synthesized as already reported [33]. Their sequences are listed in Table S1. Reagents for peptide synthesis were from Iris Biotech (Germany), solvents for peptide synthesis and HPLC analyses were from Romil (Dublin, Ireland); reversed phase columns for peptide analysis and the LC-MS was LTQ XL mass spectrometry system (Thermo Scientific, Waltham, MA) equipped with a HESI source operating at a needle voltage of 3.5 kV and at a temperature of 275 °C. The formation of lactam bridge was performed on solid support using super-acid labile protecting group, Fmoc-Lys(Mtt)-OH and Fmoc-Asp(O-2-PhiPr)-OH. These two protecting groups were removed selectively by treatment with 1% TFA, 5% triisopropylsilane (TIS) in DCM at room temperature. After the deprotection of the side chain of both lysine and aspartic acid, the coupling reaction was performed adding HATU and DIEA overnight. LC-MS analysis allowed following cyclization: by comparing chromatographic profiles, a shift in the retention times before and after cyclization of both cycles is observable, due to an increment of hydrophobicity of the cyclic forms. Peptides' purity and identity were confirmed by LC-MS (Fig. S12) and then they were lyophilized and stored at −20 °C until use.

4.2. Microscale thermophoresis experiments

MST experiments were performed with a Monolith NT 115 system (Nano Temper Technologies) equipped with 60% LED and 40% IR-laser power. Labeling of His-tagged Catalytic Domain of JAK2 (residues 826−1132) (Carna Biosciences) was achieved with the His-Tag labeling Kit RED-tris-NTA, as already reported [56]. Internal cyclic peptides were used starting from a stock solution of 1 mM in labeling buffer (Nano Temper Technologies); the dye concentration was adjusted to 100 nM while the protein concentration was 200 nM. Subsequently, 100 μL of protein and 100 μL of dye were incubated in the dark for 30 min. To monitor binding of cyclic analogues, a serial dilution (1:1) [57] was carried out by preparing 16 samples on average. Standard capillaries were employed for analysis, at 25 °C in 50 mM Tris-HCl, 150 mM NaCl,

0.05% Brij35, 1 mM DTT, 10% glycerol, at pH 7.5. An equation implemented by the software MO-S002 MO Affinity Analysis, provided by the manufacturer, was used for fitting data at different concentrations.

4.3. Circular Dichroism (CD) spectroscopy

CD spectra were recorded on a Jasco J-810 spectropolarimeter (JASCO Corp, Milan, Italy), at 25 °C in the far UV region from 190 to 260 nm. To each spectrum (averaged on three scans) related blanks were subtracted, and the signal was reported as mean residue ellipticity in units of deg* cm^2*$dmol^{-1}$*res^{-1}. All peptides were analyzed at 100 μM in 10 mM phosphate buffer at pH 7.0 and with a 0.1 cm path-length quartz cuvette [58]. While CD signal variation upon increasing temperature was evaluated at 400 μM in the same solvent system.

4.4. NMR spectroscopy

A Varian Unity Inova 600 MHz spectrometer equipped with a cold probe was implemented to acquire NMR experiments that were all registered at 298 K.

To prepare the NMR samples, internal cyclic PS5 and internal cyclic PS5 Nal1 peptides (1.2 mg each) were dissolved in 600 μL of a mixture H_2O/D_2O (99.9% D, Sigma Aldrich, Milan, Italy) 90/10 v/v. To achieve peptide conformational analyses the following NMR spectra were recorded: 2D [^{1}H, ^{1}H] TOCSY (Total Correlation Spectroscopy) [40], NOESY (Nuclear Overhauser Enhancement Spectroscopy) [42], ROESY (Rotating frame Overhauser Enhancement Spectroscopy) [41] and DQFCOSY (Double Quantum-Filtered Correlated Spectroscopy) [59]. Typical acquisition parameters were as follows: 16–64 scans, 128–256 FIDs in t1, 1024 or 2048 data points in t2. TOCSY experiments were recorded with 70 ms mixing time, NOESY experiments with 300 ms mixing time, and ROESY experiments with 250 ms time. Water suppression was accomplished through *Excitation Sculpting* [60]. Proton resonance assignments were obtained with a canonical strategy [43]. TSP (Trimethylsilyl-3-propionic acid sodium salt-D4, 99% D, Armar Scientific, Switzerland) was used as internal standard for chemical shifts referencing (0.0 ppm).

Spectra were processed with VNMRJ 1.1D (Varian, Italy) and analyzed with the software NEASY [61] contained in CARA (http://www.nmr.ch/).

NMR structures of internal cyclic PS5 and internal cyclic PS5 Nal1 were calculated using CYANA 2.1 [44]. Distance constraints were generated from 2D [^{1}H, ^{1}H] ROESY 250 spectra, and angular constraints with the GRIDSEARCH module of CYANA. The non-standard amino acids Cys(Acm) and Nal1 were added to the CYANA standard residue library. Values of the atomic coordinates were obtained from Chimera where the residues were built, and energy minimized. Asp^1 and Lys^9 side chains in both peptides were also modified in the CYANA library to allow the linkage between the CG of Asp and the NZ of Lys. The distance between Asp^1 CG and Lys^9 NZ atoms was imposed equal to 1.33 Å during structure calculations. Internal cyclic PS5 structures were generated from 92 ROE upper distance limits (67 intra-residues, 22 short-, 0 medium- and 3 long-range), including the distance constraint that was inserted for Asp^1-Lys^9 linkage, and 39 angular constraints. Internal cyclic PS5 Nal1 were generated from 146 NOE upper distance limits (117 intra-residues, 26 short-, 0 medium- and 3 long-range), including the distance constraint that was inserted for Asp^1-Lys^9 linkage, and 32 angular constraints. Calculations started from 100 random conformers, then 20 structures, provided with the lowest CYANA target functions were subjected to further unrestrained energy minimizations that were carried out with the software UCSF Chimera (version 1.10.1) [45]. Peptides minimizations were achieved through 1000 steps of steepest descent and 1000 steps of conjugate gradients. Structures were finally inspected with the programs MOLMOL [62] and PROCHECK NMR [63]. In Chimera the structures were clusterized by matching in all residues of the 20 NMR conformers, excluding N-terminal acetylation and C-terminal amidation. For further detail about Chimera clusterization protocol see Ref. [46].

4.5. Computational methods

Protein Preparation: JAK2 (PDB: 3FUP [48], chain A) missing atoms and residues were reconstructed with Swiss Model [64], as well as SOCS1 (PDB: 6C7Y [47], chain B). The complex JAK2/SOCS1 was constructed by aligning both the reconstructed JAK2 and SOCS1 to the JAK1/SOCS1 complex (PDB: 6C7Y [47]) with Swiss PDB Viewer [65]. JAK2/KIR was extracted from this complex. The JAK2/KIR complex was then minimized by performing a steepest descent minimization to be stopped either when the maximum force was lower than 1000.0 kJ/mol/nm or when 50000 minimization steps were performed with 0.005 kJ/mol energy step size, with Verlet cutoff scheme, short-range electrostatic cut-off and van der Waals cut-off of 1.0 nm. We used GROMOS 54a7 force field [66] and run the minimization as implemented in the Gromacs package v. 2016.1 [67].

Peptides preparation and docking: Ligands structures obtained by NMR were first minimized with AM1 method as implemented in MOPAC [68]. The minimized peptides were docked to the KIR binding site on JAK2 with AutoDock Vina [64]. The docking cubic box was (22.5 × 19.5 × 22.5)Å side and centered on KIR in the minimized JAK2/KIR complex (as identified by AutoDock tools). The docking was performed with exhaustiveness 500 and energy range 50. Larger exhaustiveness ad energy ranges led to the same result.

Molecular Dynamics Simulations: We placed the complex in a cubic box and minimized the complex by first minimizing protein side chains, then the entire protein and finally the whole complex by constraining selected portions of the system [69]. We then solvated the system with a water layer of 0.7 nm and performed a second minimization. We used GROMOS 54a7 force field [66] and Simple Point Charge water. Ligand topologies were built with ATB (Automated Topology Builder) [70]. We performed NVT and NPT equilibrations for 100 ps, followed by 150 ns NPT production run at 300 K. The iteration time step was set to 2 fs with the Verlet integrator and LINCS [71] constraint. We used periodic boundary conditions. All the simulations and their analysis were run as implemented in the Gromacs package v. 2016.1 [67]. RMSDs and RMSF have been calculated from configurations sampled every 10ps and as running averages over 100 sampled points. AutoDock Vina scorings were calculated over configurations sampled every 100 ps and as running averages over 10 points. Before running the simulations, the missing force field parameters were built with ATB [70]. Minimized molecular geometry led to a RMSD of 0.02896 nm for internal cyclic PS5 and 0.02535 nm for PS5 Nal1 with respect to the semi-empirical quantum chemistry minimization, thus validating the ATB-generated force field parameters. The binding free energy was estimated with the MM/PBSA method, with the apolar solvation energy calculated as solvent accessible surface area (SASA) and default parameters, as implemented in the g_mmpbsa tool [72]. Simulations were run on Marconi (CINECA, Italy).

4.6. Serum stability of peptides

These assays were performed in triplicate. 25% fetal calf serum was incubated at 37 °C for at least 15 min, then peptides were added to the serum at a concentration of 80 μM. 50 μL aliquots of

the incubating mixtures were recovered at different times: 0, 3, 17, 20, 23 and 42 h. Samples were treated with 50 μL of 15% trichloroacetic acid (TCA) and incubated at 2 °C for at least 15 min to precipitate serum proteins. The samples were subsequently centrifuged to remove serum proteins. Reverse phase high performance liquid chromatography (RP-HPLC) was performed on a HPLC 1200 series (Agilent Technologies) with UV detector using a C18 column from ThermoFisher (Milan, Italy). Gradient elution was performed at 25 °C (monitoring at 215 nm) in a gradient starting with buffer A (0.1% TFA in water) and applying buffer B (0.1% TFA in acetonitrile) from 5 to 70% in 20 min.

4.7. Cell cultures

The isolation of primary VSMCs from mouse aorta were obtained following an enzymatic digestion with collagenase type II. Cells were cultured in Dulbecco's Modified Eagle Medium (DMEM) with 10% FBS, 100 U/mL penicillin, 100 μg/mL streptomycin, and 2 mM L-glutamine (Sigma-Aldrich) and used between the 3rd and 8th passages. Mouse macrophage cell line RAW264.7 (ATCC) was maintained in DMEM supplemented with 10% FBS, 100 U/mL penicillin, 100 μg/mL streptomycin, and 2 mM L-glutamine (Sigma-Aldrich). VSMC and RAW264.7 cells were rendered quiescent by incubation in medium with 0.5% FBS and 0% FBS, respectively. Then, cells were pre-treated for 90 min with 25 μM of peptides conjugated to Tat-derived cell-penetrating sequence, before stimulation with recombinant cytokines (IFNγ 10^3 U/mL plus IL-6 10^2 U/mL; PeproTech) for different time periods.

4.8. Viability and proliferation assays

The cell viability and proliferation were determined by 3-(4,5-dimethylthiazol-2-yl)-2,5-diphenyltetrazolium bromide tetrazolium (MTT) assay. In the cell viability assay, VSMCs were seeded in 96-well plates (1×10^4 cells/well) and allowed to attach overnight at 37 °C, then incubated overnight in medium with 0.5% FBS. Peptides (25 μM) were added to the plate and incubated for additional 6 or 24 h in DMEM containing 0.5% FBS. MTT solution was then added for 2 h, and the absorbance of the metabolized MTT was measured at $\lambda = 600$ nm in a plate reader. In the cell proliferation assay, VSMCs (5×10^3 cells/well) were treated similarly except that peptides were incubated for 24 h in medium containing 10% FBS.

4.9. Wound healing assay

VSMCs were plated in 12-well plates (3×10^5 cells/well), cultured until 90–95% confluence and then depleted overnight in medium with 0.5% FBS. Scratches were then made using a sterile 200-μl pipette tip, and cells were incubated with cytokines in the presence or absence of peptides. To determine the closing speed of the wound, two images of each well were captured at different stimulation times (0, 3, 19, 26 and 45 h), the cell-free area was quantified (Image Pro-Plus; Media Cybernetics) and normalized with respect to the initial time. These assays were performed in triplicate.

4.10. Real time PCR analysis

TRI reagent (Molecular Research Center) was used to extract total RNA from cultured cells, and then complementary DNA was produced via reverse transcription. Gene expressions of *Ccl2*, *Ccl5*, *Cxcl10*, *Nox1*, *Nox4*, *Sod1* and *Cat* were analyzed by quantitative real-time polymerase chain reaction (PCR; Applied Biosystem) and mRNA values were normalized to housekeeping gene 18S expression.

4.11. Protein expression analysis

Cells were lysed in ice-cold buffer (150 mM NaCl containing 1% Triton X-100, 10 mM Tris pH 7.4, 0.5% NP-40, 1 mM EDTA, 1 mM EGTA, 0.2 mM Na_3VO_4, 0.2 mM PMSF, 10 mM NaF, and protease inhibitor cocktail). Total proteins (25 μg) were electrophoresed, transferred onto polyvinylidene fluoride membranes, and immunoblotted for phosphorylated STAT1 (pSTAT1; Invitrogen), phosphorylated JAK2 (pJAK; Invitrogen) and α-tubulin (loading control; Sigma-Aldrich) using appropriate peroxidase-conjugated secondary antibodies and chemiluminescent substrate.

4.12. Immunofluorescence studies

The VSMCs were plated on slides with 4 cameras treated for cell growth. Cells were treated for 90min with TAMRA-conjugated peptides before 1 h-stimulation, then fixed (4% paraformaldehyde), permeabilized (0.5% Triton X-100) and incubated overnight with pSTAT1 primary antibody, followed by FITC-secondary antibody (Sigma-Aldrich) and nuclear counterstaining with diamidino-2-phenylindole (DAPI). The samples were mounted using FluorSave and a confocal fluorescent microscope (Leica) was used to capture images.

4.13. DHE assay

VSMCs and RAW264.7 cells were plated on coverslips and then incubated with the fluorescent dye dihydroethidium (DHE) at 2.5 μM in KRB-HEPES buffer, for 30 min at 37 °C. After several washes to remove excess of fluorescent probe, cells were stimulated and then fixed with 1.5% paraformaldehyde, contrasted with DAPI and mounted. Fluorescence microscopy ($\lambda_{exc} = 488$ nm and $\lambda_{em} = 585$ nm) was used to analyze the samples. Intracellular $O2^{\bullet -}$ levels were expressed as number of DHE positive cells vs total cells (nuclear staining with DAPI).

4.14. Statistical analysis

Results are presented as individual data, mean ± standard error of the mean (SEM) of determinations from at least 3 independent experiments. Statistical analysis was performed using Prism 5 (GraphPad Software Inc) and differences between groups were considered significant at $p < 0.05$ (two-tailed Student's *t*-test or one-way ANOVA with Bonferroni's *post-hoc* test).

Author contributions

S.L.M., performed chemical synthesis, CD and MST assays, S.L.M., L.L. S, S. B cellular experiments, F. M., M. L. NMR experiments and solution structure calculations, S. F, computational analysis, D. M. and C G. G. conceived, designed experiments and analyzed data. D.M. wrote the manuscript with the contributions of all authors. All authors have given approval to the final version of the manuscript.

Funding sources

This work was partially supported by POR CAMPANIA FESR 2014/2020 “Combattere la resistenza tumorale: piattaforma integrata multidisciplinare per un approccio tecnologico innovativo alle oncoterapie-Campania Oncoterapie” (Project N. B61G18000470007). C.G-G was supported by Spanish Ministry of Science, Innovation and Universities (MICINN/FEDER, RTI2018-098788-B-I00) and Ministry of Health (FIS, DTS17/00203 and DTS19/00093).

Declaration of competing interest

The authors declare that they have no known competing financial interests or personal relationships that could have appeared to influence the work reported in this paper.

Acknowledgment

We acknowledge the CINECA Award N. HP10CRVL7F, 2017, for the availability of high-performance computing resources and support. Sara La Manna was supported by the AIRC fellowship for Italy.

Abbreviations

ATB	Automated Topology Builder
Biotin-SA	Biotin-streptavidin
CAT	catalase
CCL	C-C motif chemokine ligand
CXCL	C-X-C motif chemokine ligand
CD	Circular Dichroism
Cys(Acm)	Acetaminomethyl-L-cysteine
DHE	Dihydroethidium
DQFCOSY	Double Quantum-Filtered Correlated Spectroscopy
EDTA	Ethylenediaminetetraacetic acid
EGTA	Egtazic acid
ESS	Extended SH2 Subdomain
FBS	Fetal Bovine Serum
Hepes	4-(2-hydroxyethyl)-1-piperazineethanesulfonic acid
ICAM-1	Intercellular Cell Adhesion Molecule-1
INF-γ	Interferon gamma
IL	Interleukin
JAK	Janus Kinases
KIR	Kinase Inhibitory Region
LC-MS	Liquid Chromatography Mass Spectrometry
MD	molecular dynamics
MM/PBSA	Molecular Mechanics/Poisson-Boltzmann Solvent-Accessible Surface Area
MST	Microscale Thermophoresis
Nal	Naphtylalanine
NC	Negative Control
NMR	Nuclear Magnetic Resonance
NOESY	Nuclear Overhauser Enhancement Spectroscopy
PCR	Polymerase Chain Reaction
PMSF	Phenylmethylsulfonyl Fluoride
RMSD	Root Mean Square Deviation
RMSF	Root Mean Squared Fluctuation
ROESY	Rotating Frame Overhauser Enhancement Spectroscopy
SH2	Src Homology 2
SOCS	Suppressors Of Cytokine Signaling
SOD1	superoxide dismutase 1
STAT	Signal Transducer and Activator of Transcription
TAMRA	Tetramethylrhodamine
TCA	Trichloroacetic acid
TNF-α	Tumor Necrosis Factor α
TOCSY	Total Correlation Spectroscopy
TSP	Trimethylsilyl-3-propionic acid sodium salt-D4
VSMCs	Vascular smooth muscle cells

References

[1] W.S. Alexander, D.J. Hilton, The role of suppressors of cytokine signaling (SOCS) proteins in regulation of the immune response, Annu. Rev. Immunol. 22 (2004) 503–529.
[2] B.A. Croker, H. Kiu, S.E. Nicholson, SOCS regulation of the JAK/STAT signalling pathway, Semin. Cell Dev. Biol. 19 (2008) 414–422.
[3] A. Yoshimura, T. Naka, M. Kubo, SOCS proteins, cytokine signalling and immune regulation, Nat. Rev. Immunol. 7 (2007) 454–465.
[4] E.M. Linossi, J.J. Babon, D.J. Hilton, S.E. Nicholson, Suppression of cytokine signaling: the SOCS perspective, Cytokine Growth Factor Rev. 24 (2013) 241–248.
[5] D.L. Krebs, R.T. Uren, D. Metcalf, S. Rakar, J.G. Zhang, R. Starr, D.P. De Souza, K. Hanzinikolas, J. Eyles, L.M. Connolly, R.J. Simpson, N.A. Nicola, S.E. Nicholson, M. Baca, D.J. Hilton, W.S. Alexander, SOCS-6 binds to insulin receptor substrate 4, and mice lacking the SOCS-6 gene exhibit mild growth retardation, Mol. Cell Biol. 22 (2002) 4567–4578.
[6] M.R.G. Santos, C.M. Queiroz-Junior, M.F.M. Madeira, F.S. Machado, Suppressors of cytokine signaling (SOCS) proteins in inflammatory bone disorders, Bone 140 (2020) 115538.
[7] S. Huang, K. Liu, A. Cheng, M. Wang, M. Cui, J. Huang, D. Zhu, S. Chen, M. Liu, X. Zhao, Y. Wu, Q. Yang, S. Zhang, X. Ou, S. Mao, Q. Gao, Y. Yu, B. Tian, Y. Liu, L. Zhang, Z. Yin, B. Jing, X. Chen, R. Jia, SOCS proteins participate in the regulation of innate immune response caused by viruses, Front. Immunol. 11 (2020) 558341.
[8] H.M. Johnson, A.S. Lewin, C.M. Ahmed, SOCS, intrinsic virulence factors, and treatment of COVID-19, Front. Immunol. 11 (2020) 582102.
[9] A. Yoshimura, T. Ohkubo, T. Kiguchi, N.A. Jenkins, D.J. Gilbert, N.G. Copeland, T. Hara, A. Miyajima, A novel cytokine-inducible gene CIS encodes an SH2-containing protein that binds to tyrosine-phosphorylated interleukin 3 and erythropoietin receptors, EMBO J. 14 (1995) 2816–2826.
[10] J.J. Babon, L.N. Varghese, N.A. Nicola, Inhibition of IL-6 family cytokines by SOCS3, Semin. Immunol. 26 (2014) 13–19.
[11] N.P.D. Liau, A. Laktyushin, I.S. Lucet, J.M. Murphy, S. Yao, E. Whitlock, K. Callaghan, N.A. Nicola, N.J. Kershaw, J.J. Babon, The molecular basis of JAK/STAT inhibition by SOCS1, Nat. Commun. 9 (2018) 1558.
[12] S.E. Nicholson, T.A. Willson, A. Farley, R. Starr, J.G. Zhang, M. Baca, W.S. Alexander, D. Metcalf, D.J. Hilton, N.A. Nicola, Mutational analyses of the SOCS proteins suggest a dual domain requirement but distinct mechanisms for inhibition of LIF and IL-6 signal transduction, EMBO J. 18 (1999) 375–385.
[13] W.S. Alexander, R. Starr, J.E. Fenner, C.L. Scott, E. Handman, N.S. Sprigg, J.E. Corbin, A.L. Cornish, R. Darwiche, C.M. Owczarek, T.W. Kay, N.A. Nicola, P.J. Hertzog, D. Metcalf, D.J. Hilton, SOCS1 is a critical inhibitor of interferon gamma signaling and prevents the potentially fatal neonatal actions of this cytokine, Cell 98 (1999) 597–608.
[14] J.E. Fenner, R. Starr, A.L. Cornish, J.G. Zhang, D. Metcalf, R.D. Schreiber, K. Sheehan, D.J. Hilton, W.S. Alexander, P.J. Hertzog, Suppressor of cytokine signaling 1 regulates the immune response to infection by a unique inhibition of type I interferon activity, Nat. Immunol. 7 (2006) 33–39.
[15] G.M. Davey, R. Starr, A.L. Cornish, J.T. Burghardt, W.S. Alexander, F.R. Carbone, C.D. Surh, W.R. Heath, SOCS-1 regulates IL-15-driven homeostatic proliferation of antigen-naive CD8 T cells, limiting their autoimmune potential, J. Exp. Med. 202 (2005) 1099–1108.
[16] J.L. Eyles, D. Metcalf, M.J. Grusby, D.J. Hilton, R. Starr, Negative regulation of interleukin-12 signaling by suppressor of cytokine signaling-1, J. Biol. Chem. 277 (2002) 43735–43740.
[17] T. Tamiya, I. Kashiwagi, R. Takahashi, H. Yasukawa, A. Yoshimura, Suppressors of cytokine signaling (SOCS) proteins and JAK/STAT pathways regulation of T-cell inflammation by SOCS1 and SOCS3, Arterioscl. Throm. Vas. 31 (2011) 980–985.
[18] S. Madonna, C. Scarponi, O. De Pita, C. Albanesi, Suppressor of cytokine signaling 1 inhibits IFN-gamma inflammatory signaling in human keratinocytes by sustaining ERK1/2 activation, Faseb. J. 22 (2008) 3287–3297.
[19] R. Balabanov, K. Strand, R. Goswami, E. McMahon, W. Begolka, S.D. Miller, B. Popko, Interferon-gamma-oligodendrocyte interactions in the regulation of experimental autoimmune encephalomyelitis, J. Neurosci. 27 (2007) 2013–2024.
[20] J.N. Ihle, B.A. Witthuhn, F.W. Quelle, K. Yamamoto, O. Silvennoinen, Signaling through the hematopoietic cytokine receptors, Annu. Rev. Immunol. 13 (1995) 369–398.
[21] S. Ilangumaran, S. Ramanathan, R. Rottapel, Regulation of the immune system by SOCS family adaptor proteins, Semin. Immunol. 16 (2004) 351–365.
[22] J. Hadjadj, C.N. Castro, M. Tusseau, M.C. Stolzenberg, F. Mazerolles, N. Aladjidi, M. Armstrong, H. Ashrafian, I. Cutcutache, G. Ebetsberger-Dachs, K.S. Elliott, I. Durieu, N. Fabien, M. Fusaro, M. Heeg, Y. Schmitt, M. Bras, J.C. Knight, J.C. Lega, G. Lesca, A.L. Mathieu, M. Moreews, B. Moreira, A. Nosbaum, M. Page, C. Picard, T. Ronan Leahy, I. Rouvet, E. Ryan, D. Sanlaville, K. Schwarz, A. Skelton, J.F. Viallard, S. Viel, M. Villard, I. Callebaut, C. Picard, T. Walzer, S. Ehl, A. Fischer, B. Neven, A. Belot, F. Rieux-Laucat, Early-onset autoimmunity associated with SOCS1 haploinsufficiency, Nat. Commun. 11 (2020) 5341.
[23] C.M. Ahmed, J. Larkin 3rd, H.M. Johnson, SOCS1 mimetics and antagonists: a complementary approach to positive and negative regulation of immune function, Front. Immunol. 6 (2015) 183.
[24] C. Recio, A. Oguiza, I. Lazaro, B. Mallavia, J. Egido, C. Gomez-Guerrero,

Suppressor of cytokine signaling 1-derived peptide inhibits Janus kinase/signal transducers and activators of transcription pathway and improves inflammation and atherosclerosis in diabetic mice, Arterioscler. Thromb. Vasc. Biol. 34 (2014) 1953–1960.
[25] L. Lopez-Sanz, S. Bernal, C. Recio, I. Lazaro, A. Oguiza, A. Melgar, L. Jimenez-Castilla, J. Egido, C. Gomez-Guerrero, SOCS1-targeted therapy ameliorates renal and vascular oxidative stress in diabetes via STAT1 and PI3K inhibition, Lab. Invest. 98 (2018) 1276–1290.
[26] L. Opazo-Rios, Y. Sanchez Matus, R.R. Rodrigues-Diez, D. Carpio, A. Droguett, J. Egido, C. Gomez-Guerrero, S. Mezzano, Anti-inflammatory, antioxidant and renoprotective effects of SOCS1 mimetic peptide in the BTBR ob/ob mouse model of type 2 diabetes, BMJ Open Diabet. Res. Care 8 (2020).
[27] C. Recio, I. Lazaro, A. Oguiza, L. Lopez-Sanz, S. Bernal, J. Blanco, J. Egido, C. Gomez-Guerrero, Suppressor of cytokine signaling-1 peptidomimetic limits progression of diabetic nephropathy, J. Am. Soc. Nephrol. : JASN (J. Am. Soc. Nephrol.) 28 (2017) 575–585.
[28] C. He, C.R. Yu, M.J. Mattapallil, L. Sun, J. Larkin Iii, C.E. Egwuagu, SOCS1 Mimetic Peptide Suppresses Chronic Intraocular Inflammatory Disease (Uveitis), vol. 2016, Mediators of inflammation, 2016, p. 2939370.
[29] C.M. Ahmed, M.T. Massengill, E.E. Brown, C.J. Ildefonso, H.M. Johnson, A.S. Lewin, A cell penetrating peptide from SOCS-1 prevents ocular damage in experimental autoimmune uveitis, Exp. Eye Res. 177 (2018) 12–22.
[30] S. Bernal, L. Lopez-Sanz, L. Jimenez-Castilla, I. Prieto, A. Melgar, S. La Manna, J.L. Martin-Ventura, L.M. Blanco-Colio, J. Egido, C. Gomez-Guerrero, Protective effect of suppressor of cytokine signalling 1-based therapy in experimental abdominal aortic aneurysm, Br. J. Pharmacol. 178 (3) (2020) 564–581.
[31] S. Madonna, C. Scarponi, N. Doti, T. Carbone, A. Cavani, P.L. Scognamiglio, D. Marasco, C. Albanesi, Therapeutical potential of a peptide mimicking the SOCS1 kinase inhibitory region in skin immune responses, Eur. J. Immunol. 43 (2013) 1883–1895.
[32] N. Doti, P.L. Scognamiglio, S. Madonna, C. Scarponi, M. Ruvo, G. Perretta, C. Albanesi, D. Marasco, New mimetic peptides of the kinase-inhibitory region (KIR) of SOCS1 through focused peptide libraries, Biochem. J. 443 (2012) 231–240.
[33] S. La Manna, L. Lopez-Sanz, M. Leone, P. Brandi, P.L. Scognamiglio, G. Morelli, E. Novellino, C. Gomez-Guerrero, D. Marasco, Structure-activity Studies of Peptidomimetics Based on Kinase-Inhibitory Region of Suppressors of Cytokine Signaling 1, Biopolymers, 2017.
[34] S. La Manna, L. Lopez-Sanz, S. Bernal, L. Jimenez-Castilla, I. Prieto, G. Morelli, C. Gomez-Guerrero, D. Marasco, Antioxidant effects of PS5, a peptidomimetic of suppressor of cytokine signaling 1, in: Experimental Atherosclerosis, vol. 9, 2020. Antioxidants (Basel).
[35] D. Marasco, G. Perretta, M. Sabatella, M. Ruvo, Past and future perspectives of synthetic peptide libraries, Curr. Protein Pept. Sci. 9 (2008) 447–467.
[36] E. Lonardo, C.L. Parish, S. Ponticelli, D. Marasco, D. Ribeiro, M. Ruvo, S. De Falco, E. Arenas, G. Minchiotti, A small synthetic cripto blocking Peptide improves neural induction, dopaminergic differentiation, and functional integration of mouse embryonic stem cells in a rat model of Parkinson's disease, Stem Cell. 28 (2010) 1326–1337.
[37] S. Ponticelli, D. Marasco, V. Tarallo, R.J. Albuquerque, S. Mitola, A. Takeda, J.M. Stassen, M. Presta, J. Ambati, M. Ruvo, S. De Falco, Modulation of angiogenesis by a tetrameric tripeptide that antagonizes vascular endothelial growth factor receptor 1, J. Biol. Chem. 283 (2008) 34250–34259.
[38] D. Meyer, C. Mutschler, I. Robertson, A. Batt, C. Tatko, Aromatic interactions with naphthylalanine in a beta-hairpin peptide, J. Pept. Sci. 19 (2013) 277–282.
[39] R. Oliva, M. Chino, K. Pane, V. Pistorio, A. De Santis, E. Pizzo, G. D'Errico, V. Pavone, A. Lombardi, P. Del Vecchio, E. Notomista, F. Nastri, L. Petraccone, Exploring the role of unnatural amino acids in antimicrobial peptides, Sci. Rep. 8 (2018) 8888.
[40] C. Griesinger, G. Otting, K. Wuthrich, R.R. Ernst, Clean tocsy for H-1 spin system-identification in macromolecules, J. Am. Chem. Soc. 110 (1988) 7870–7872.
[41] A. Bax, D.G. Davis, Practical aspects of two-dimensional transverse noe spectroscopy, J. Magn. Reson. 63 (1985) 207–213.
[42] A. Kumar, R.R. Ernst, K. Wuthrich, A two-dimensional nuclear Overhauser enhancement (2D NOE) experiment for the elucidation of complete proton-proton cross-relaxation networks in biological macromolecules, Biochem. Biophys. Res. Commun. 95 (1980) 1–6.
[43] K. Wuthrich, in: NMR of Proteins and Nucleic Acids, Wiley, New York, 1986.
[44] T. Herrmann, P. Guntert, K. Wuthrich, Protein NMR structure determination with automated NOE assignment using the new software CANDID and the torsion angle dynamics algorithm DYANA, J. Mol. Biol. 319 (2002) 209–227.
[45] E.F. Pettersen, T.D. Goddard, C.C. Huang, G.S. Couch, D.M. Greenblatt, E.C. Meng, T.E. Ferrin, UCSF Chimera–a visualization system for exploratory research and analysis, J. Comput. Chem. 25 (2004) 1605–1612.
[46] L.A. Kelley, S.P. Gardner, M.J. Sutcliffe, An automated approach for clustering an ensemble of NMR-derived protein structures into conformationally related subfamilies, Protein Eng. 9 (1996) 1063–1065.
[47] N.P. Liau, A. Laktyushin, I.S. Lucet, J.M. Murphy, S. Yao, E. Whitlock, K. Callaghan, N.A. Nicola, N.J. Kershaw, J.J. Babon, The molecular basis of JAK/STAT inhibition by SOCS1, Nat. Commun. 9 (2018) 1558.
[48] N.K. Williams, R.S. Bamert, O. Patel, C. Wang, P.M. Walden, A.F. Wilks, E. Fantino, J. Rossjohn, I.S. Lucet, Dissecting specificity in the Janus kinases: the structures of JAK-specific inhibitors complexed to the JAK1 and JAK2 protein tyrosine kinase domains, J. Mol. Biol. 387 (2009) 219–232.
[49] F. Giordanetto, R.T. Kroemer, A three-dimensional model of suppressor of cytokine signalling 1 (SOCS-1), Protein Eng. 16 (2003) 115–124.
[50] H.Y. Chow, Y. Zhang, E. Matheson, X. Li, Ligation Technologies for the synthesis of cyclic peptides, Chem. Rev. 119 (2019) 9971–10001.
[51] A. Russo, C. Aiello, P. Grieco, D. Marasco, Targeting "undruggable" proteins: design of synthetic cyclopeptides, Curr. Med. Chem. 23 (2016) 748–762.
[52] I.F. Charo, R. Taub, Anti-inflammatory therapeutics for the treatment of atherosclerosis, Nat. Rev. Drug Discov. 10 (2011) 365–376.
[53] E.P. Demina, V. Smutova, X. Pan, A. Fougerat, T. Guo, C. Zou, R. Chakraberty, B.D. Snarr, T.C. Shiao, R. Roy, A.N. Orekhov, T. Miyagi, M. Laffargue, D.C. Sheppard, C.W. Cairo, A.V. Pshezhetsky, Neuraminidases 1 and 3 trigger atherosclerosis by desialylating low-density lipoproteins and increasing their uptake by macrophages, J. Am. Heart Assoc. 10 (2021), e018756.
[54] G.Y. Kim, H. Jeong, H.Y. Yoon, H.M. Yoo, J. Lee, S.H. Park, C.E. Lee, Anti-inflammatory mechanisms of suppressors of cytokine signaling target ROS via NRF-2/thioredoxin induction and inflammasome activation in macrophages, BMB Rep. 53 (12) (2020) 640–645.
[55] L.L. Sanz, S. Bernal, I. Lazaro, L.J. Castilla, A. Melgar, J. Egido, C.G. Guerrero, SOCS1-based therapies mitigate vascular and renal oxidative stress in diabetic mice through STAT1-and PI3K-dependent mechanisms, Atherosclerosis 275 (2018) e50.
[56] F.A. Mercurio, C. Di Natale, L. Pirone, R. Iannitti, D. Marasco, E.M. Pedone, R. Palumbo, M. Leone, The Sam-Sam interaction between Ship2 and the EphA2 receptor: design and analysis of peptide inhibitors, Sci. Rep. 7 (2017) 17474.
[57] F.A. Mercurio, D. Marasco, C. Di Natale, L. Pirone, S. Costantini, E.M. Pedone, M. Leone, Targeting EphA2-sam and its interactome: design and evaluation of helical peptides enriched in charged residues, Chembiochem : Eur. J. Chem. Biol. 17 (2016) 2179–2188.
[58] P.L. Scognamiglio, C. Di Natale, M. Leone, R. Cascella, C. Cecchi, L. Lirussi, G. Antoniali, D. Riccardi, G. Morelli, G. Tell, F. Chiti, D. Marasco, Destabilisation, Aggregation, Toxicity and Cytosolic Mislocalisation of Nucleophosmin Regions Associated with Acute Myeloid Leukemia, Oncotarget, 2016.
[59] U. Piantini, O.W. Sorensen, R.R. Ernst, Multiple quantum filters for elucidating NMR coupling networks, J. Am. Chem. Soc. 104 (1982) 6800–6801.
[60] T.L. Hwang, A.J. Shaka, Water suppression that works - excitation sculpting using arbitrary wave-forms and pulsed-field gradients, J. Magn. Reson., Ser. A 112 (1995) 275–279.
[61] C. Bartels, T.H. Xia, M. Billeter, P. Guntert, K. Wuthrich, The program XEASY for computer-supported NMR spectral analysis of biological macromolecules, J. Biomol. NMR 6 (1995) 1–10.
[62] R. Koradi, M. Billeter, K. Wuthrich, MOLMOL: a program for display and analysis of macromolecular structures, J. Mol. Graph. 14 (51–55) (1996) 29–32.
[63] R.A. Laskowski, J.A. Rullmannn, M.W. MacArthur, R. Kaptein, J.M. Thornton, AQUA and PROCHECK-NMR: programs for checking the quality of protein structures solved by NMR, J. Biomol. NMR 8 (1996) 477–486.
[64] A. Waterhouse, M. Bertoni, S. Bienert, G. Studer, G. Tauriello, R. Gumienny, F.T. Heer, T.A.P. de Beer, C. Rempfer, L. Bordoli, SWISS-MODEL: homology modelling of protein structures and complexes, Nucleic Acids Res. 46 (2018) W296–W303.
[65] N. Guex, M.C. Peitsch, SWISS-MODEL and the Swiss-Pdb Viewer: an environment for comparative protein modeling, Electrophoresis 18 (1997) 2714–2723.
[66] N. Schmid, A.P. Eichenberger, A. Choutko, S. Riniker, M. Winger, A.E. Mark, W.F. van Gunsteren, Definition and testing of the GROMOS force-field versions 54A7 and 54B7, Eur. Biophys. J. 40 (2011) 843.
[67] S. Pronk, S. Páll, R. Schulz, P. Larsson, P. Bjelkmar, R. Apostolov, M.R. Shirts, J.C. Smith, P.M. Kasson, D. van der Spoel, GROMACS 4.5: a high-throughput and highly parallel open source molecular simulation toolkit, Bioinformatics 29 (2013) 845–854.
[68] J.J.P. Stewart, Special issue - MOPAC - a semiempirical molecular-orbital program, J. Comput. Aided Mol. Des. 4 (1990) 1–45.
[69] E.R. Lindahl, Molecular dynamics simulations, Methods Mol. Biol. 443 (2008) 3–23.
[70] A.K. Malde, L. Zuo, M. Breeze, M. Stroet, D. Poger, P.C. Nair, C. Oostenbrink, A.E. Mark, An automated force field Topology builder (ATB) and repository: version 1.0, J. Chem. Theor. Comput. 7 (2011) 4026–4037.
[71] B. Hess, H. Bekker, H.J. Berendsen, J.G. Fraaije, LINCS: a linear constraint solver for molecular simulations, J. Comput. Chem. 18 (1997) 1463–1472.
[72] R. Kumari, R. Kumar, O.S.D.D. Consortium, A. Lynn, g_mmpbsa- A GROMACS tool for high-throughput MM-PBSA calculations, J. Chem. Inf. Model. 54 (2014) 1951–1962.